Ocean Engineering 259 (2022) 111893

Contents lists available at ScienceDirect

Ocean Engineering

journal homepage: www.elsevier.com/locate/oceaneng

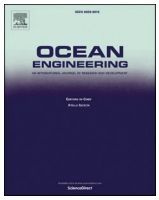

A new method for optimal ship design in real sea states using the ship power profile

Ehsan Esmailian *, Sverre Steen

Department of Marine Technology, Norwegian University of Science and Technology (NTNU), Trondheim, Norway

ARTICLE INFO

Keywords:
Ship design
Optimization
Real sea states
Ship power profile
Rough sea

ABSTRACT

Typically, ships are designed for calm water and a constant design speed. However, a ship experiences different speeds and sea conditions over her lifetime. Following the significant correlations between environment and ship behavior at sea, efforts are needed to design energy-efficient and safe ships with good performances in realistic sea conditions. This article proposes a method for optimization of the design of a ship with respect to different levels of propulsive power and different operational conditions using a probabilistic approach. The objective of the optimization is the average ship speed, averaged over all propulsion power and environmental condition combinations based on a long-term analysis. The proposed approach is tested on a Post-Panamax container ship operating in the route from Busan to Hamburg port. The decision variables are the ship and propeller main dimensions. Comparisons with traditional methods used in ship design are also presented. Comparing the proposed method with the traditional methods indicates that 7.89% increase in average ship speed is obtained, demonstrating that the proposed method is effective in designing better ships for actual sea states. Better performance in rough sea for the ship designed with the proposed method is also reported.

1. Introduction

The shipping industry has a key position in the global economy as it carries out about 90% of the world's transport. Since greenhouse gas (GHG) emissions from ships are expected to increase by 50−250% by 2050 (Smith et al., 2014), the International Maritime Organization (IMO) set environmental regulations forcing the ship designers to find more effective and reliable methods for mitigating GHG emissions from ships.

The IMO initial plans are to reduce total annual GHG emissions by 50% by 2050, while lowering carbon intensity (CI) by 40% by 2030 and decarbonizing up to 70% by 2050 in a business-as-usual scenario (Resolution, 2018). To reach these goals, the shipping industry must seek solutions to improve the energy efficiency of ships, lower the CI of new ships and improve the Energy Performance Index (EEDI) as quickly as possible (Joung et al., 2020).

From calm water to real sea, the ship performance varies considerably. Due to the effect of the environmental factors, mostly wind and waves, ships experience higher resistances and slower forward speeds in real sea states.

Traditionally, ship designers have assessed hydrodynamic performance by looking at calm water resistance. In recent years, there has been a growing attention on the effect of added resistance on the ship efficiency. Bolbot and Papanikolaou (2016) incorporated added resistance, calm water resistance, total resistance, and EEDI to optimize the bow shape of a KVLCC2 vessel. In (Bolbot and Papanikolaou, 2016), sectional area curves and section shapes in the design load waterline of a 66,000 DWT bulk carrier are adjusted to optimize both the wave-making resistance and the added resistance in waves. Jung & Kim (Jung and Kim, 2019) undertook an optimization study based on the total resistance and the speed loss in waves, taking into account the main dimensions of KVLCC2 tankers as the optimization decision variables. The method suggested in that study led to up to 13.9% reductions in total resistance. In (Kim et al., 2021), the hull form optimization is carried out in order to minimize both total resistance and speed loss of an VLCC tanker operating under representative sea conditions. It was shown that the brake power required by the ship under representative sea conditions is reduced by 4.61%. A 66, 000 DWT bulk carrier with a sharp bow form compares favorably to a blunt bow form in (Lee et al., 2019), for both calm water and waves. It was found that the pressure component of resistance in the sharp bow is decreased by 8.9% in calm water, and by 6.4% and 12.7% in regular head waves.

Depending on the weather and the ship schedule, a ship will operate

* Corresponding author.
E-mail addresses: ehsan.esmailian@ntnu.no (E. Esmailian), sverre.steen@ntnu.no (S. Steen).

https://doi.org/10.1016/j.oceaneng.2022.111893
Received 17 September 2021; Received in revised form 26 May 2022; Accepted 2 July 2022
Available online 16 July 2022

Nomenclature

A_e/A_o	expanded area ratio
A_{xv}	transverse projected area
B	ship beam
C_{AA}	wind resistance coefficient
$C^{Q}_{s,t,u,v}$	regression coefficient for torque
$C^{T}_{s,t,u,v}$	regression coefficient for thrust
C_B	block coefficient
CSR	Continuous service rating
d	ship draft
D_p	propeller diameter
em	engine margin
g	gravity acceleration
GM	metacentric height
GZ	righting lever
H	ship depth
H_s	significant wave height
J	advance coefficient
K_Q	torque coefficient
K_T	thrust coefficient
L_{pp}	Length between perpendiculars
LCG	longitudinal center of gravity
LOA	overall length
MCR	engine's nominal maximum continuous rating
MEP	mean effective pressure
m_n	total number of probability variables
n	rotational rate
$n_{Head_{leg}}$	number of the heading angles for a given voyage leg
n_{leg}	number of voyage legs over the entire voyage
N_{SMCR}	engine speed at the SMCR power
$n_{Wave_{leg}}$	numbers wave angles for a given voyage leg
$n_{Zone_{leg}}$	number of zones contributing a give voyage leg
n_{Zone}	the number of zones contributing a given route
$P_{\theta_{Wave_{leg}}}$	probability of wave angle for a given voyage leg
$P_{\theta_{Zone}}$	probability of wave angle for a given zone
$P_{b_{Cal}}$	calculated engine power
$P_{b_{Opr}}$	operation engine power
$P_{b_{SMCR}}$	brake power at the SMCR point
$\overline{P}_{Cav}$	probability of cavitation
$P_{Enc_{leg}}$	probability of the encountered wave angle for a voyage leg
P^{tot}_{Enc}	encounter wave probability for the entire voyage
$P_{Head_{leg}}$	probability of ship heading for a given voyage leg
P_{hrDes}	brake power for the heavy running at the design speed
P_P	probability of power
P_{SD}	probabilities of different significant wave heights and peak wave periods
$P_{Time_{leg}}$	probability of a voyage leg over the entire voyage
$P_{Zone_{leg}}$	contribution of a zone to a given voyage leg
P_{Zone}	contribution of a zone over the entire route
P_0	atmospheric pressure
P_b	brake power
P/D_p	pitch ratio
PC	percentage change
P_E	effective power
P_s	shaft power
pm	propeller margin
P_V	vapor pressure
$\overline{Pr}_{Cav}$	cavitation probability in percent
P_{trDes}	brake power for the trial condition at the design speed
R_{AW}	mean added resistance in irregular waves
R_{aw}	added resistance due to wave
R_{Calm}	calm water resistance
$\overline{R}_{Calm}$	average calm water resistance over the long term
R_{Wind}	added resistance due to the wind
R_T	total resistance
$\overline{R}_T$	average total resistance over the long term
s	power coefficient
SS	sea state
S	wave spectrum
SD_{wave}	wave scatter
SD^{route}_{wave}	wave scatter for a given route
sm	sea margin
$SMCR$	specified maximum continuous rating
t	power coefficient
T_p	peak wave period
T_C	calculated thrust
t_p	thrust deduction factor
T_R	required thrust
u	power coefficient
v	power coefficient
V_A	mean axial advance velocity
V_d	design speed
V_G	ship's speed over ground
V_S	ship forward speed
$\overline{V}_S$	average speed over the long term
V_{WRref}	relative wind velocity at the reference height
V_{WTref}	corrected true wind velocity
KG	vertical center of gravity
w	wake fraction
Z	number of blades
z_G	vertical center of gravity above the waterline
β	encounter wave angle
Δ	ship displacement
Δ_0	parent ship displacement
η_G	transmission efficiency
η_H	hull efficiency
η_o	open water efficiency
η_R	relative rotative efficiency
η_S	shaft efficiency
η_T	total propulsive efficiency
∇	ship displacement volume
ω	wave frequency
ψ	ship heading
ψ_{WRref}	relative wind direction at the reference height
ψ_{WT}	true wind direction
ρ_{air}	air density
$\theta_{Head_{leg}}$	ship headings for a given voyage leg
$\theta_{Wave_{leg}}$	wave angle for a given voyage leg
θ_{Zone}	wave angle of a given zone
ζ_a	wave amplitude

at different speeds. As a result, designing a ship for a single design speed might lead to sub-optimal designs. In the literature, some steps towards the development of ship design methods at sea are presented in (Peri et al., 2001; Campana et al., 2006; Serani et al., 2014; Hart and Vlahopoulos, 2010), but only at a single design speed.

In several studies, probabilistic approaches have been suggested for the optimal design of ships in terms of the operational envelope. In (Temple and Collette, 2012), a probability mission profile based on the ship speed was employed to examine the tradeoffs between resistance and production complexity. In the study carried out in (Esmailian et al.,

2017), simultaneous optimization of a Series-60 ship hull with a B-series propeller was suggested to minimize the ship's lifetime fuel consumption (LFC) based on a probabilistic ship speed profile. A study conducted in (Esmailian et al., 2019) suggested the use of an integrated photovoltaic system to optimize the design of a boat based upon the probabilistic ship speed profile. In (Kramer et al., 2010), a probabilistic approach combining speed and sea-state was applied to maximize the efficiency of a waterjet through optimizing the diameter. It was found that probabilistic approaches improved life-cycle efficiency by between 3 and 10%. Using a similar probabilistic approach, Motley et al. (Motley and Young, 2011) investigated the advantages of self-adaptive composite propellers over nickel-aluminum-bronze propellers. Motley et al. (2012) suggested a probability-based approach for minimizing LFC of marine propulsors. Based on the optimization of the hull-propeller system of a KCS container ship, LFC was minimized via a probabilistic speed approach (Nelson et al., 2013).

Further, if a ship has not been properly designed with respect to the total operational envelope, she might experience considerable power load and speed losses and fluctuations, which can substantially affect the performances and life cycles of both mechanical and electrical systems (Perez et al., 2006; Sørensen and Smogeli, 2009; Smogeli and Sørensen, 2009). From the mechanical system point of view, these will increase mechanical stress and thus wear and tear (Smogeli, 2006; Radan, 2008; Smogeli et al., 2008). The power fluctuations can also negatively affect the electrical systems through reductions in electrical efficiency, unpredictable power consumption, and even power quality on the shipboard power network (Sørensen and Smogeli, 2009; Smogeli and Sørensen, 2009; Radan, 2008; Smogeli et al., 2008).

If one observes the operation of a ship over a prolonged period of time, like several weeks or more, one will see that both speed and power vary considerably, and one will observe that they (of course) are closely correlated. Thus, when taking a probabilistic approach to ship design, one can choose to use either a speed profile or a power profile to represent the probability of each speed or power level. However, one might also observe that speed and sea state are correlated, so that higher sea states usually lead to lower speeds. This is less clear for power, since power tends to be kept relatively constant regardless of weather, until conditions for voluntary speed reductions are reached. The different stochastic variables in a probabilistic approach should ideally not be correlated (or else the correlation must be accounted for, which is difficult). Therefore, this study uses a power profile instead of a speed profile to represent the variation in operating point of the ship. The resulting speed is instead a calculated result variable, being a function of both the ship design and the weather condition, in addition to the input power.

The present study proposes a new methodology for the optimal design with respect to propulsion of ships in the actual weather considering the ship power profile. The suggested approach aims to assess whether at the same power profile more energy-efficient designs with better behaviors at sea can be achieved. Consequently, we aim to design ships with the highest average attainable speed with the given power profile, resulting in more energy-efficient ships at sea.

In the following section, we will describe the methodology applied for predicting the ship performance in terms of the average speed over the long term. In section 3, the proposed method in implemented on a ship design problem. Section 4 describes the results. Finally, the conclusion is presented in section 5 with an overview of this research and a few directions for future research.

2. Ship performance evaluation method

In this section, the methods applied to calculate the ship resistance, propulsion system efficiency and the cavitation criterion are discussed first. Then, the strategy applied to determine probabilities of power, sea state and wave and wind directions used in the suggested method are presented. Finally, the proposed methodologies used to calculate the average ship speed over the long term and the resistance criterion are explained.

2.1. Resistance

The ship total resistance is divided into three components as follows.

$$R_T = R_{Calm} + R_{AW} + R_{Wind} \tag{1}$$

where R_{Calm} is the calm water resistance, R_{AW} is the added resistance in waves, and R_{Wind} is the added resistance due to the wind.

2.1.1. Calm water resistance

As a better estimation, the mean value of the calm water resistances was calculated from two well-known methods, Holtrop and Mennen (1984) (Holtrop, 1984) and Hollenbach (1998), is taken. These methods are widely used to calculate the calm water resistance of ships for a wide range of sizes, hull forms, and Froude numbers. For Hollenbach's approach, the mean line of resistance is applied.

The AHR (average hull roughness) of a new ship is between 75 and 125 μm (Stewart, 2008). In computing the calm water resistance, AHR = 150 μm is considered in this study-including the effects of fouling-which is the standard value recommended by ITTC when there is no measured data (Yeginbayeva and Atlar, 2018).

2.1.2. Added resistance in waves

Added resistance depends on both the weather and the ship speed, and thus a wide range of wave periods, wave heights, wave directions, and ship speeds experienced by the ship needs to be consider for a better estimation. In this study, the formula given by Liu and Papanikolaou called the SHOPERA-NTUA-NTU-MARIC (SNNM) method is applied (Liu and Papanikolaou, 2020; Wang et al., 2021), which is a semi-empirical formula to calculate the added wave resistance at arbitrary wavelength, heading, and draft. That approach was adopted through improving the asymptotic formula given by Faltinsen (1980) to capture the diffraction effect and the empirical method developed by Jinkine and Ferdinande (1974) to include the effect of the radiation.

The mean added resistance in the irregular waves is estimated by numerical integration of a series of regular waves with frequency ω and wave amplitude ζ_a for a particular wave heading, significant wave height H_s and the peak wave period T_p and is expressed as

$$R_{AW} = 2\int_0^{2\pi}\int_0^{\infty} S(\omega)\,\frac{R_{aw}(\omega,\beta,V_S)}{\zeta_a^2}\,d\omega\,d\beta \tag{2}$$

where S, β, and V_S are the wave spectrum, the encounter wave angle and the ship forward speed, respectively. R_{aw} is the added resistance computed according to Liu and Papanikolaou's method. Additionally, for the fully developed sea, we employ the Bretschneider wave spectrum expressed as follows.

$$S(\omega) = \frac{A_{fw}}{\omega^5} exp\left(\frac{-B_{fw}}{\omega^4}\right) \tag{3}$$

where

$$A_{fw} = 173\frac{H_s^2}{T_p^4} \tag{4}$$

and

$$B_{fw} = \frac{692}{T_p^4} \tag{5}$$

2.2. Wind resistance

The wind resistance is calculated by the formula given by ISO 15016-2015 as follows (ISO, 2015).

$$R_{wind} = 0.5\rho_{air}\cdot C_{AA}(\psi_{WRref})\cdot A_{xv}\cdot V_{WRref}^2 - 0.5\rho_{air}\cdot C_{AA}(0)\cdot A_{xv}\cdot V_G^2 \quad (6)$$

where R_{wind} is the resistance increase due to relative wind, ρ_{air} is the density of air, A_{xv} is the transverse projected area above the waterline including superstructures, $C_{AA}(\psi_{WRref})$ is the wind resistance coefficient, wherein ψ_{WRref} is the relative wind direction at the reference height (usually 10 m above the free surface), V_G is the ship's speed over ground, and V_{WRref} is the relative wind velocity at the reference height, as defined in Fig. 1. C_{AA} depends on the vessel type and heading, and it is found based on data presented in (ISO, 2015) for a container ship. V_{WRref} is written as

$$V_{WRref} = \sqrt{V_{WTref}^2 + V_s^2 + 2\cdot V_{WTref}\cdot Vs\cdot cos(\psi_{WT} - \psi)} \quad (7)$$

where V_{WTref} denotes the corrected true wind velocity in meters per second, ψ_{WT} is the true wind direction in degrees and ψ is the ship heading in degrees. It is assumed that wind and wave have the same direction. Hence, $\beta = \psi_{WT} - \psi$. Also, the wind speed V_{WTref} is (Stewart, 2008)

$$V_{WTref} = \sqrt{\frac{gH_s}{0.22}} \quad (8)$$

2.3. Propulsion system

For the B-series propellers (Oosterveld and van Oossanen, 1975), the thrust coefficient, K_T, and the torque coefficient, K_Q, are given by

$$K_T = \Sigma C^T_{s,t,u,v}(J)^s\left(\frac{P}{D_p}\right)^t\left(\frac{A_e}{A_o}\right)^u(Z)^v \quad (9)$$

$$K_Q = \Sigma C^Q_{s,t,u,v}(J)^s\left(\frac{P}{D_p}\right)^t\left(\frac{A_e}{A_o}\right)^u(Z)^v \quad (10)$$

where $C^Q_{s,t,u,v}$ and $C^T_{s,t,u,v}$ are the regression coefficients and s, t, u, and v are the power coefficients. Also, J, $\frac{P}{D_p}$, $\frac{A_e}{A_o}$ and Z denote the advance coefficient, the pitch ratio, the blade expanded area ratio, and the number of blades, respectively.

The operational performance of a marine propeller is largely dependent on the advance coefficient, J, which is expressed by the mean axial advance velocity, V_A, the rotational speed of the propeller, n, and the propeller diameter, D_p, as follows.

$$J = \frac{V_A}{nD_p} \quad (11)$$

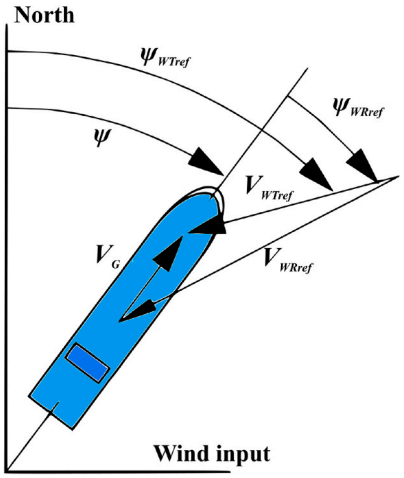

Fig. 1. Coordinate system for calculating added resistance in winds.

where V_A is found by

$$V_A = V_S(1 - w) \quad (12)$$

where w is the wake fraction. Also, the open water efficiency is given by

$$\eta_o = \frac{K_T J}{K_Q 2\pi}. \quad (13)$$

In the design process of the propeller, the calculated thrust T_C need to be equal to the required thrust T_R. The propeller thrust and the required thrust can be calculated by

$$T_C = K_T\rho n^2 D_p^4, \quad (14)$$

$$T_R = \frac{R_T}{1 - t_p} \quad (15)$$

where t_p is the thrust deduction fraction. Then, K_T is used in calculations as follows.

$$K_T = \frac{T_R}{\rho n^2 D_p^4} = AJ^2 \quad (16)$$

where A is defined by

$$A = \frac{T_R}{\rho V_A^2 D_p^2}. \quad (17)$$

Knowing the ship resistance, wake fraction and thrust deduction fraction, the parameter A can be calculated at each ship speed. Then, the advance coefficient and corresponding propeller open water efficiency, η_o, are calculated by finding the intersection point between $K_T(J)$ given by the propeller open water diagram and $K_T(J)$ obtained by (16).

The impact of the hull on the propeller can be measured by the relative rotative efficiency η_R and the wake fraction w. The former represents the change in propeller efficiency in comparison to the open water condition and the latter describes the change in inflow velocity. The propeller effect on the hull is captured by the thrust deduction fraction t_p. In the absence of model tests, those parameters were estimated using the formulas provided by Holtrop and Mennen (Holtrop, 1984).

The required effective power is expressed by

$$P_E = R_T U \quad (18)$$

Also, the required brake power, P_b, is given by

$$P_b = \frac{P_E}{\eta_T} \quad (19)$$

with

$$\eta_T = \eta_H\eta_o\eta_R\eta_S \quad (20)$$

where η_H is the hull efficiency; η_R is the relative rotative efficiency; and η_S is the shaft efficiency. Therefore, once R_T and η_T are obtained, P_b can be calculated through (19) at each ship speed.

2.4. Cavitation constraint

Cavitation negatively affects propeller performance and can destroy propellers, rudders, or any other nearby surfaces. By increasing the blade area ratio, propeller cavitation can be minimized, at the cost of reduced propeller efficiency. In this study, the Keller's approach is employed to estimate the minimum blade area ratio to avoid cavitation as follows.

$$A_E \Big/ A_{o_{min}} = \frac{(1.3 + 0.3Z)T_R}{(P_0 - P_V)D_p^2} + K \quad (21)$$

where the constant $K = 0.2$, 0.1 and 0 for single, slow twin and fast twin-

screw vessels, respectively. Also, P_0 and P_V are the atmospheric and vapor pressures, respectively.

2.5. Engine limits

The operating point of an engine is determined using load and layout diagrams. The engine layout diagram specifies the engine design point for a given engine. It consists of four points -R_1, R_2, R_3, and R_4, which are illustrated in Fig. 2 as an example. The R_1 point represents the engine's nominal maximum continuous rating (MCR) which is defined as the engine's maximum continuous power at the engine's maximum continuous rotation rate. Upper and lower border lines, i.e. $R_1 - R_3$ and $R_2 - R_4$, specify the upper and lower mean effective pressure (MEP) limits for the design point, respectively.

Continuous service rating (CSR) refers to the point in which an engine's fuel efficiency is at its peak, typically between 70 and 80 percent of the engine load. Furthermore, the specified maximum continuous rating (SMCR) is the maximum combination of power and speed produced by the ship's engine as installed, including effects such as coupling with the propeller and tuning for the application. The SMCR point, defined by the brake power, $P_{b_{SMCR}}$, and the rotation rate, N_{SMCR}. $P_{b_{SMCR}}$ is defined as

$$P_{b_{SMCR}} = P_{hrDes}(1 + em) \tag{22}$$

Specifically, em represents the engine margin, typically 10%, and P_{hrDes} is the brake power for heavy running at the design speed. In this study, when the engine limits for calm water conditions are examined, P_{hrDes} is derived as follows.

$$P_{hrDes} = P_{trDes}(1 + sm) \tag{23}$$

where P_{trDes} is trial running power, defining the brake power for the trial condition at the design speed. In addition, sm denotes the sea margin. Depending on the ship type and the operating area, the sea margin varies, however, the typical value of 15% is assumed in this research.

N_{SMCR} represents the engine speed at the SMCR power, N_{hrDes}, decreased by the propeller margin, pm, which is set to 5% here, such that

$$N_{SMCR} = N_{hrDes}(1 - pm). \tag{24}$$

Accordingly, the following engine limits are considered (MAN Energy Solutions, 2018):

- Engine Operating Limit. According to this limit, the propeller curves for entire operating ranges of the engine in different sea states and speeds must fall within the engine load diagram defined by the engine's speed, power, mean effective pressure, and torque limits, as illustrated in Fig. 2.
- SMCR Limit. Based on this limit, the SMCR point must fall within the layout diagram. Otherwise, a different propeller speed or engine type must be chosen.

2.6. Probabilistic mission profile

In this chapter, how to compute the probabilities P_{Enc}^{tot}, P_{SD}, and P_P are explained.

2.6.1. Probability of power

A ship power profile is defined as a probability density function (PDF) representing the likelihood that the ship will operate at different power levels over her operational envelope. It is highly dependent on the type of vessel and can be derived through assessing in-service data of a similar ship with the same mission or by some other knowledge of how the ship is expected to operate. The power profile is an important input to the design process, and it might be of interest to look at how different power profiles influence the finally optimized ship. As an example, Fig. 3 shows the ship profile for a 13100 TEU class container ship operating as a liner in the route from Pusan to Hamburg ports, that is derived from the ship in-service data.

2.6.2. Probabilities of significant wave height and mean wave period

A reliable description of the sea conditions that are experienced by the ship across the long term is essential when designing a ship. Information on expected weather and ship response can be incorporated into a model to analyse the ship's performance over the long term. This requires considering the probability of different weather conditions across the navigating area. In this regard, the wave scatter diagram, which displays the probabilities of a range of significant wave heights and the mean wave periods in a grid covering a specific area, can be helpful. To estimate the scatter diagram for the ship voyage, the method suggested in (Det Norske Veritas, 2010) is applied. Accordingly, the significant wave height is presented by a three-parameter Weibull probability density function formed by a conditional modeling approach (CMA) as

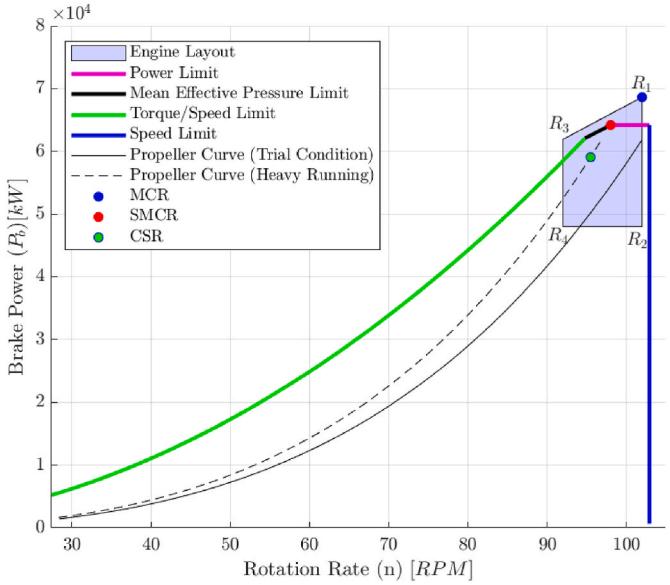

Fig. 2. Schematic engine load diagram and operating limits for a ship.

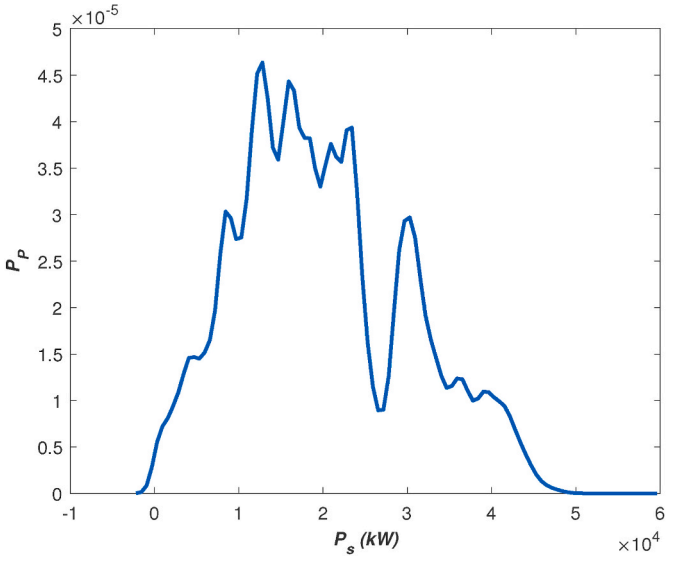

Fig. 3. Ship power profile for the 13100 TEU class container ship. Where $P_s = P_b$ as there is no gearbox.

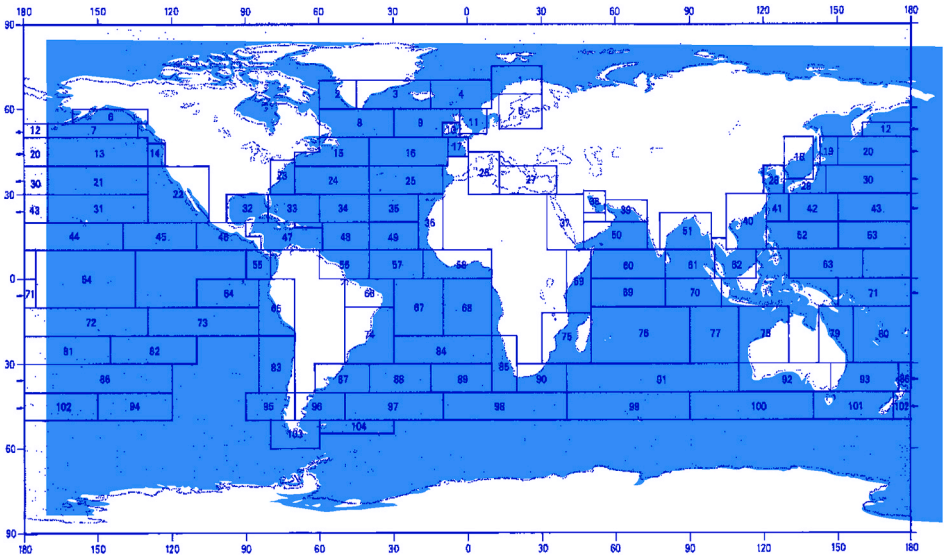

Fig. 4. Nautic zones for estimation of long-term wave distribution parameters.

$$f_{H_s}(H_s) = \frac{\beta_{H_s}}{\alpha_{H_s}}\left(\frac{H_s - \gamma_{H_s}}{\alpha_{H_s}}\right)^{\beta_{H_s}-1} \exp\left(-\frac{H_s - \gamma_{H_s}}{\alpha_{H_s}}\right)^{\beta_{H_s}} \tag{25}$$

Likewise, the peak wave period conditional on H_s as a lognormal distribution is expressed by

$$f_{T_p|H_s}(T_p|H_s) = \frac{1}{\sigma T_p\sqrt{2\pi}}\exp\left(-\frac{(lnT_p - \mu)^2}{2\sigma^2}\right) \tag{26}$$

where μ and σ are the distribution parameters and defined as

$$\mu = a_0 + a_1 H_s^{a_1} \tag{27}$$

$$\sigma = b_0 + b_1 e^{b_2 H_s} \tag{28}$$

Also, β_{H_s}, α_{H_s}, γ_{H_s}, a_m, and b_m ($m = 0$, 1, and 2) can be obtained based on the data given by (Det Norske Veritas, 2010) for different nautic zones depicted in Fig. 4. Following this, the wave scatter for an arbitrary nautic zone, SD_{wave}, is calculated as follows.

$$SD_{wave} = f_{H_s} f_{T_p|H_s} \tag{29}$$

Regarding different zones operating by the ship, the wave scatter for a given route, SD^{route}_{wave}, is given by

$$SD^{route}_{wave} = \sum_{i=1}^{n_{Zone}} P^i_{Zone} SD^i_{wave} \tag{30}$$

where n_{Zone} is the number of zones contributing to a given route. In addition, P^i_{Zone} is calculated based on the contribution of each zone to the entire voyage. Having the ship scatter diagram over her route, one will be able to obtain the probabilities of different significant wave heights and peak wave periods $P_{SD}(H_S, T_p)$ experienced by the ship within her operations.

2.6.3. Probability of wind and wave encounter angles

To estimate the probability of the encounter wave angle for the entire ship voyage, the probability of the wave angles for different voyage legs are obtained first. The data given by (Det Norske Veritas, 2010) is used to determine the wave angles θ_{Zone} and their corresponding probabilities $P_{\theta_{Zone}}$ for the zones depicted in Fig. 4. Then, regarding the contribution of each zone to each voyage leg, $P_{Zone_{leg}}$, the wave angle $\theta_{Wave_{leg}}$ and its corresponding probability $P_{\theta_{Wave_{leg}}}$ for a given voyage leg are computed as follows.

$$\theta_{Wave_{leg}} = \sum_{i=1}^{n_{Zone_{leg}}} P^i_{Zone_{leg}} \theta^i_{Zone} \tag{31}$$

$$P_{\theta_{Wave_{leg}}} = \sum_{i=1}^{n_{Zone_{leg}}} P^i_{Zone_{leg}} P^i_{\theta_{Zone}} \tag{32}$$

where $n_{Zone_{leg}}$ denotes the number of zones contributing a give voyage leg.

Considering the ship route, the ship headings for a given voyage leg $\theta_{Head_{leg}}$ and their corresponding probabilities $P_{Head_{leg}}$ are calculated. Then, the probability of the encountered wave angle for a given voyage leg $P_{Enc_{leg}}$ is determined as follows.

$$P_{Enc_{leg}} = \sum_{m=1}^{n_{Head_{leg}}} \sum_{n=1}^{n_{Wave_{leg}}} P^m_{Head_{leg}} P^n_{\theta_{Wave_{leg}}} (\theta^m_{Head_{leg}} - \theta^n_{Wave_{leg}}) \tag{33}$$

where $n_{Head_{leg}}$ and $n_{Wave_{leg}}$ are the numbers of the heading and wave angles for a given voyage leg, respectively. Finally the encounter wave probability for the entire voyage P^{tot}_{Enc} is given as follows.

$$P^{tot}_{Enc} = \sum_{k=1}^{n_{leg}} P^k_{Time_{leg}} P^k_{Enc_{leg}} \tag{34}$$

where n_{leg} is the number of voyage legs over the entire voyage. Furthermore, based on the ship time schedule, the probability of the voyage legs operating by the ship $P_{Time_{leg}}$ is estimated. As mentioned earlier, it is assumed that wind and waves are inline, i.e., $\beta = \psi_{WT} - \psi$. As a result, there is no separate probability value for wind direction. Similarly, the wind speed is dependent on the wave height as given by equation (8), so that there is no separate probability value for wind speed either.

2.7. Attainable average speed over the long term

In this section, the suggested methodology applied to calculate the attainable average speed over the long term $\overline{V}_S$ is explained. The proposed method consists of three loops, as shown in Fig. 5. In the inner loop, the ship speed corresponding to a given power and environment is calculated. Once the absolute difference between the operation engine power $P_{b_{Opr}}$ derived from the ship power profile and the calculated engine power $P_{b_{Cal}}$ calculated by the power model is less than 1% of $P_{b_{Opr}}$, the inner loop stops. Moreover, $n_{P^{tot}_{Enc}}$, $n_{P_{SD}}$, and n_{P_P} are considered as the numbers of probability values for the encounter waver angle β, the pair of H_s and T_p, and the ship brake power P_b, respectively. The middle loop ends when the total number of probability values $m_n = n_{P^{tot}_{Enc}}\ n_{P_{SD}}\ n_{P_P}$ is reached. Finally, the outer loop stops once the termination criteria for the optimization algorithm are met. Also, with regard to probability values, the average ship operational speed over the long term is

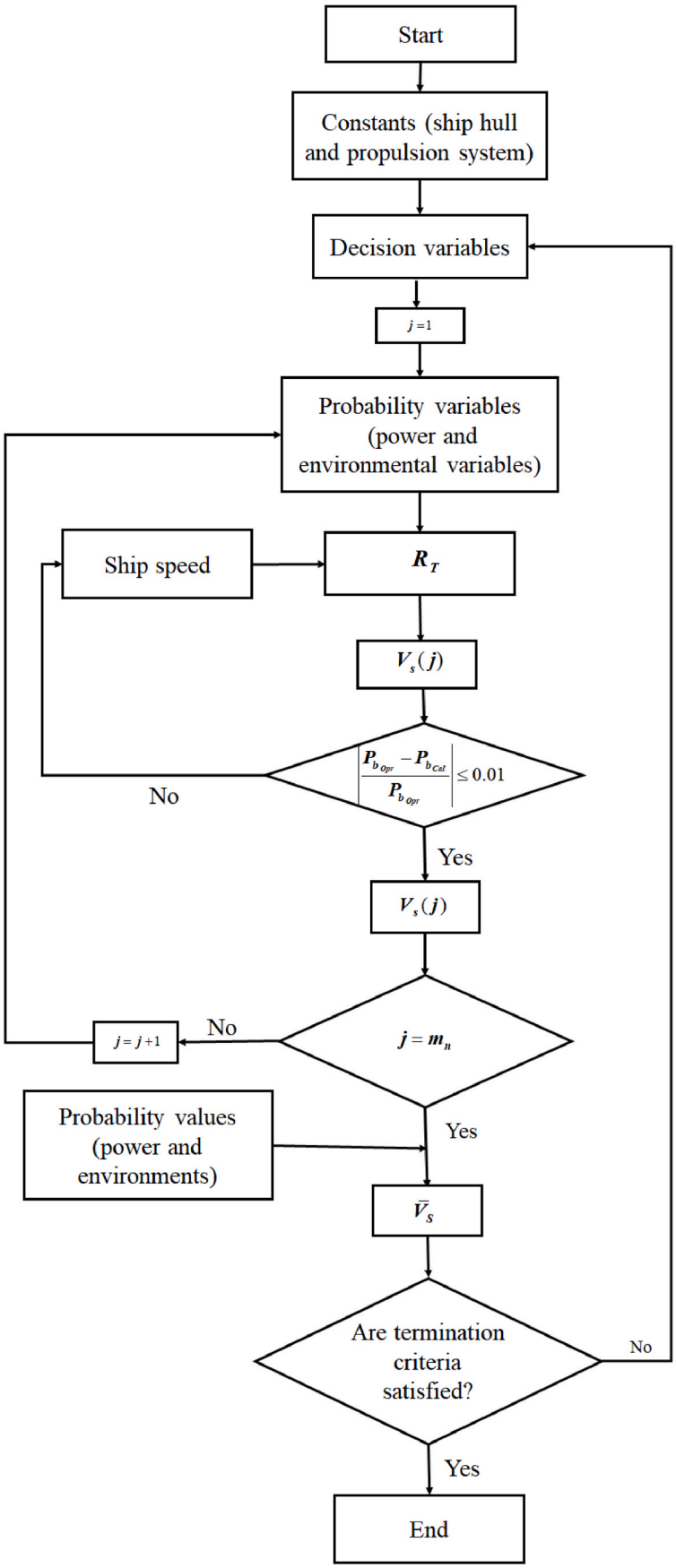

Fig. 5. Flowchart of the proposed method.

calculated as follows.

$$\overline{V_S} = \iiiint P_{Enc}^{tot}(\beta)\, P_{SD}(H_S, T_p)\, P_P(P_b)\, V_s\, d\beta\, dT_p\, dH_s\, dP_b. \quad (35)$$

In the suggested method, $\overline{V_S}$ is the optimization objective.

2.8. Resistance criterion

A trade-off analysis is also provided to assess whether a ship should be designed for a seaway, as illustrated in Fig. 6. The reason to present

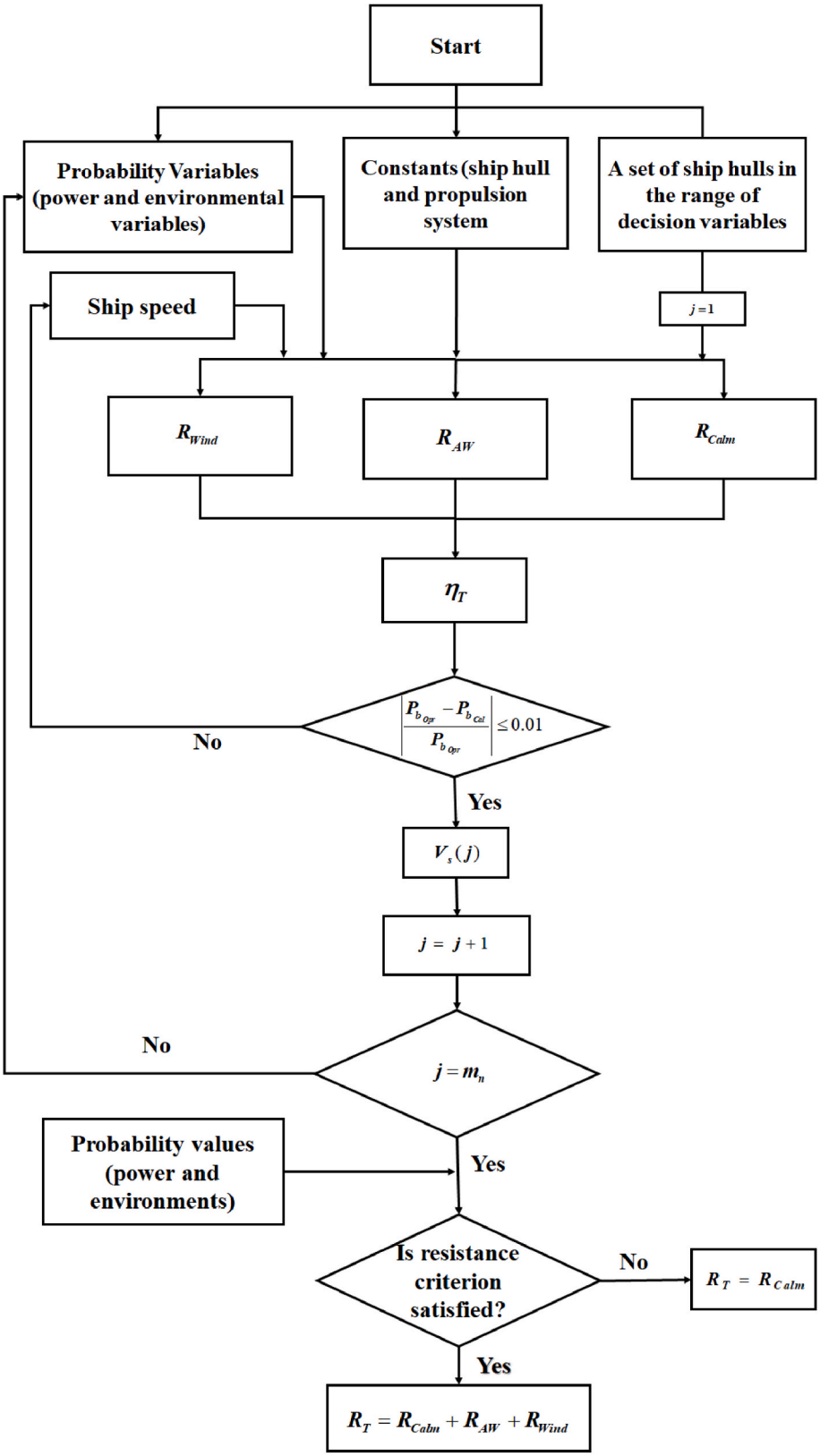

Fig. 6. Flowchart of the resistance criterion.

this analysis is that designing a ship for the real sea states will significantly increase computation time and therefore costs, as well as the general complexity of the problem. Consequently, a trade-off analysis might be helpful in assessing whether a ship needs to be designed for a seaway. Accordingly, by comparing the averaged calm water resistance with the resistance at sea for a set of ship hulls satisfying the decision variable ranges, the following criterion is suggested.

$$\frac{\sum_{k=1}^{n_{hull}} \left| \frac{\overline{R}_T - \overline{R}_{Calm}}{\overline{R}_T} \right|}{n_{hull}} \geq c \tag{36}$$

where c denotes a design limit for considering calm water resistance only and is determined by the designer. In this research, $c = 0.15$ is assumed, which is the same as the typical value for the sea margin. $\overline{R}_T$ and $\overline{R}_{Calm}$ are the average of total and calm water resistances over the long term, respectively. They are defined as follows.

$$\overline{R}_T = \iiiint P_{Enc}^{tot}(\beta)\, P_{SD}(H_S, T_p)\, P_P(P_b)\, R_T(\beta, H_S, T_p, P_b)\, d\beta\, dT_p\, dH_s\, dP_b \tag{37}$$

$$\overline{R}_{Calm} = \int P_P(P_b)\, R_{Calm}(P_b)\, dP_b \tag{38}$$

where R_T and R_{Calm} are the ship total and calm water resistances, respectively. The following sections detail the strategies used to calculate the parameters given in (35), (37), and (38).

3. Ship design problem

In this section, the proposed strategy is tested on the 14000 TEU post-panamax DTC container ship (Moctar et al., 2012) operating as a liner in the route from Pusan to Hamburg ports, as seen in Fig. 7. The main particulars of the ship are presented in Table 1. Table 2 presents different voyage legs and their corresponding $P_{Time_{leg}}$ for the studied ship. $P_{Time_{leg}}$ is the probability of a particular leg, taken as the relative amount of time spent on that leg. The Sulzer/Wärtsilä 12RTA96C engine (Aeberli, 2005) is considered for the ship similar to the studied 13100 TEU class container ship. The layout diagram for this engine is given in (Demmerle, 1997).

Through the continuous increase in the number of vessels equipped with data acquisition (DAQ) systems and onboard sensors, a wide range of parameters related to the ship performance and navigation can be measured, including ship speed, power, and fuel consumption. In this regard, there is a tremendous potential to use the ship in-service data for the new ship designs. In this study, the probability parameters ship power profile is derived by analyzing the ship in-service data of the 13100 TEU class container ship operating as a liner in the same operational route as the DTC container ship. The main particulars of the 13100 TEU class container ship are presented in Table 3. The results of the probability of the wave encounter angles for the different voyages

Table 1
Main particulars for the DTC container ship.

Parameters	Value	Unit
L_{pp}	355.0	[m]
B	51.0	[m]
d	14.5	[m]
LCG position	174.059	[m]
KG position	19.851	[m]
C_B	0.661	[−]
∇	173468	[m^3]
V_d	25	[knots]

Table 2
Different voyage legs for the studied ship.

West Bound	$P_{Time_{leg}}$[%]	East Bound	$P_{Time_{leg}}$[%]
Xingang-Kwangyang (South Korea)	2.5	Hamburg-Rotterdam (Netherland)	1.8
Kwangyang-Pusan (South Korea)	0.5	Rotterdam-Lehavre (France)	1.2
Pusan-Shanghai (China)	2.1	Lehavre-Algeciras (Spain)	5.9
Shanghai-Xiamen (China)	1.9	Algeciras-Suez (Egypt)	8.6
Xiamen-Yantian (China)	1.5	Suez-Singapore	21.3
Yantian-Singapore	5.5	Singapore-Yantian (China)	5.8
Singapore-Suez (Egypt)	19.6	Yantian-Hongkong (China)	0.3
Suez-Algeciras (Spain)	8.0	Hongkong-Xingang (China)	6.6
Algeciras-Hamburg (Germany)	6.8		

Table 3
Ship principle particulars.

Parameters	Value	Unit
LOA	360.0	[m]
L_{pp}	345.0	[m]
B	48.2	[m]
H	28.0	[m]
d	15.0	[m]
Δ	185,000	[ton]

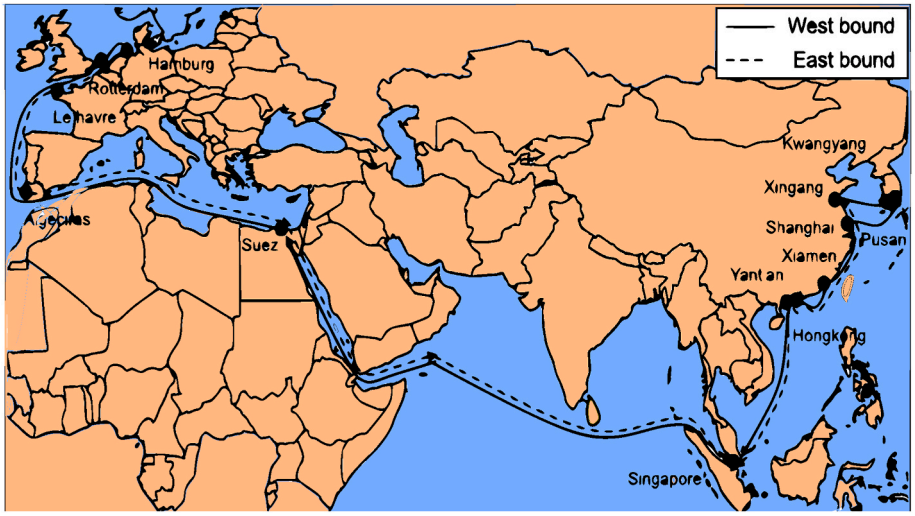

Fig. 7. The ship operational route.

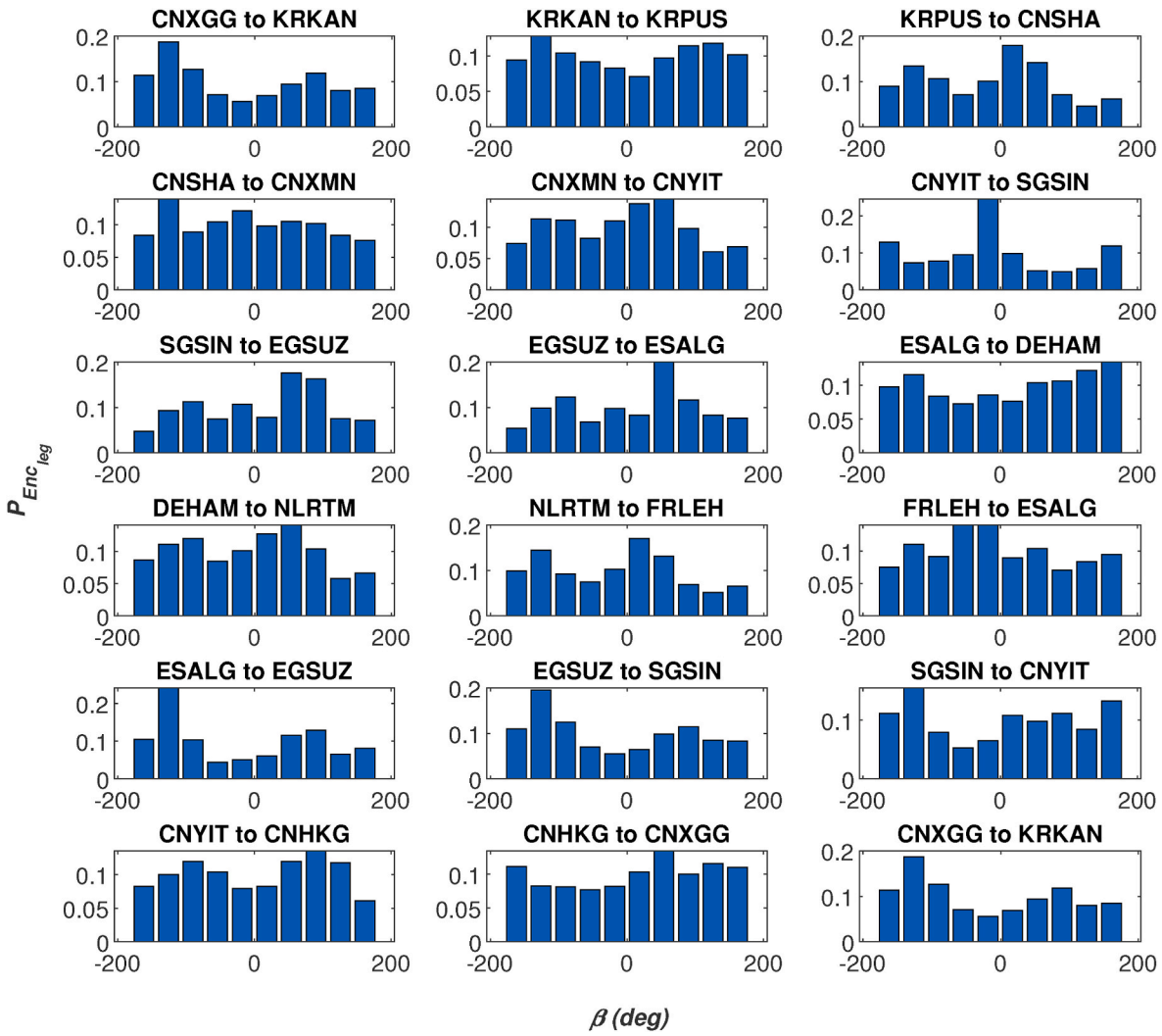

Fig. 8. Probabilities of the encounter wave angle for different ship voyage legs.

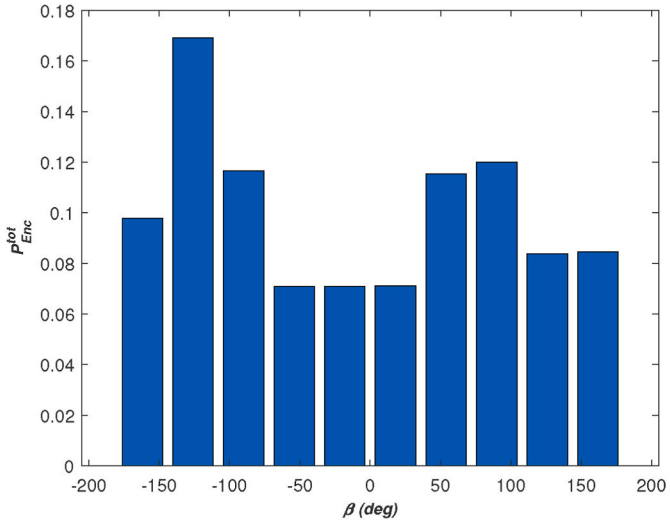

Fig. 9. Probabilities of the encounter wave angle over the entire ship voyage.

and the entire voyage are provided in Figs. 8 and 9, respectively. The obtained ship power profile is presented in Fig. 3.

3.1. Validation

A reliable model to predict propulsion power is essential for the entire design process. In this study, the methods used to calculate the ship propulsion power are validated against experimental data, numerical analyses, and ship in-service data.

3.2. Model validation in model test and full scale

In this section, the model validation is performed for the DTC container ship for both model and full-scale cases. For this purpose, a comparison for the calm water resistance results against experimental data and CFD analyses are presented in Figs. 10 and 11. In the model scale, the results of the calculation are compared with the model test data (Moctar et al., 2012) and the results of a Reynolds-averaged Navier–Stokes (RANS) solver known as SHIPFLOW XCHAP considering $k-\omega$ SST (Shear-Stress Transport) model (Larsson et al., 2020).

In the full scale, the results of calculations are compared with those of the GL Rankine solver (Gourlay et al., 2015) plus the ITTC 1978 method, along with the results of scaling the model test results. The GL Rankine solver is a potential flow code used to determine the wave resistance and the ITTC 1978 method is applied to estimate frictional

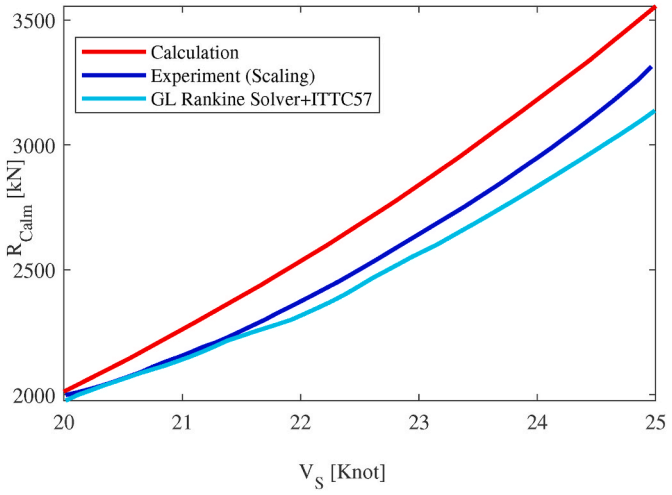

Fig. 10. Comparison of the calm water resistance for the full scale.

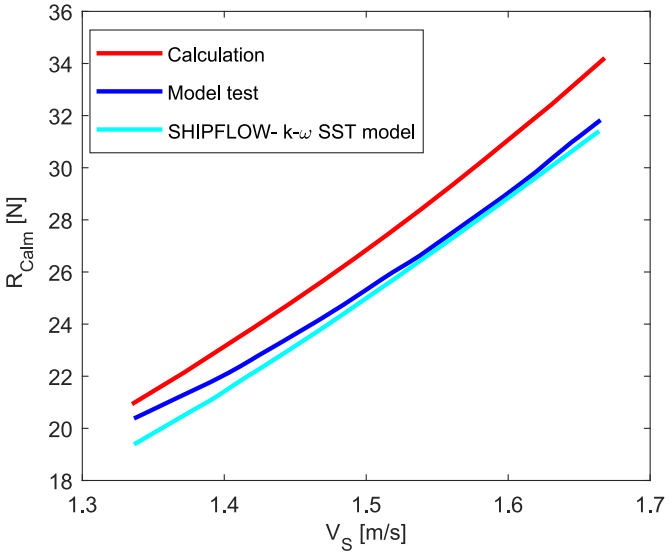

Fig. 11. Comparison of the calm water resistance for the model.

resistance. As shown in Figs. 10 and 11, there is good agreement between the different results.

In Fig. 12, the calculated added resistance in waves using the SNNM method for DTC container ship is compared to the experimental results at Fr = 0.052, indicating a good agreement between the calculated added resistance in waves and the experiment results in different wave directions. Similar results for a wide variety of ships and Froude numbers are also presented (Liu and Papanikolaou, 2020; Wang et al., 2021).

3.3. Model validation using ship service data at actual seas

Fig. 13 provides a comparison between the in-service data of the studied 13100 TEU class container ship and the power prediction model in a variety of environmental scenarios. The environment data for the studied ship has been obtained based on the data presented in (Copernicus climate change service, 2021). In the analysis, the measured speed from the in-service data is input to the power prediction model, and Fig. 13 then compares measured and calculated shaft power. The results indicate good agreement with the ship in-services data.

3.4. Optimization formulation and setting

Here, the main objective is to optimize hydrodynamically the main dimensions of the hull and propulsion system of the DTC container ship in a range of realistic operating conditions. It is worth mentioning that the proposed method is general and not limited to container ships, and our purpose here is to demonstrate the potential of the method in reducing the required power/increasing speed by optimizing the main dimensions. As a result, other design aspects, such as the internal arrangement, hull structure, machinery, safety, etc, although very important, are outside of the scope of this article. Therefore, the ship beam is treated as a continuous variable, not varied in steps of one container beam.

In order to evaluate the proposed optimization approach, a set of cases are examined, as presented in Table 4. Cases 4 and 5 reflect the traditional methods in ship design relying on the constant ship design speed.

Similar to (35), we define the averaged ship speed $\overline{V}_S$ over the entire operational range as an optimization objective for the cases 2 and 3. While Case 2 considers different environmental conditions, Case 3 applies the same power profile, but is ignoring added resistance due to weather. Case 2 is representing our proposed optimization method, while the other cases are included for the comparison. As shown by (35), (18) and (19), selecting $\overline{V}_S$ as the optimization objective also allows us to consider the effects of both ship resistance and propulsion system efficiency, together with their interactions. Further, for the cases 4 and 5, the optimization objective is the averaged ship resistance over the entire operational range, as presented in (37) and (38) for the sea and calm water conditions. Thus, for cases 4 and 5, the propeller is not optimized, but kept equal to the parent, Case 1.

The limits of decision variables are provided in Table 5, which are compatible with recommendations for decision variable ranges for designing a container ship suggested in (Nelson et al., 2013; Cepowski and Chorab, 2021; Charchalis and Krefft, 2009). The ship displacement is constrained to be within 5% of that of the parent hull. This will result in a limited variation in the number of TEUs among different cases. Since the internal arrangement is outside the scope of this paper, the actual number of containers is not calculated. Also, the ship main dimensions are affected by the topological limitations of the route, i.e., the width of canals, ports, channels, and confined waters. Considering the range of decision variables, the restrictions for the Suez Canal (Suez canal restrictions for operating, 2013) needed to be taken into account. As shown in Table 5 of the article, the requirements for the Suez Canal are satisfied by defining them as constraints in the optimization problem. The ship offset table is used to calculate the hydrostatic parameters. Therefore, the size of the ship is controlled through a quite strict limit (5%) on the displacement, as well as limitations on the other main dimensions which are less strict, but still ensure that the resulting ship hulls are realistic, and will fulfill important restrictions related to stability, ability to navigate particularly important restricted waters and so on.

Through the optimization algorithm, the ship offset is changed at each iteration to reach the optimal hull. Furthermore, the height of the ship center of gravity above the keel (KG) is calculated as the sum of the vertical center of gravity above the waterline z_G and the draft d, i.e. KG

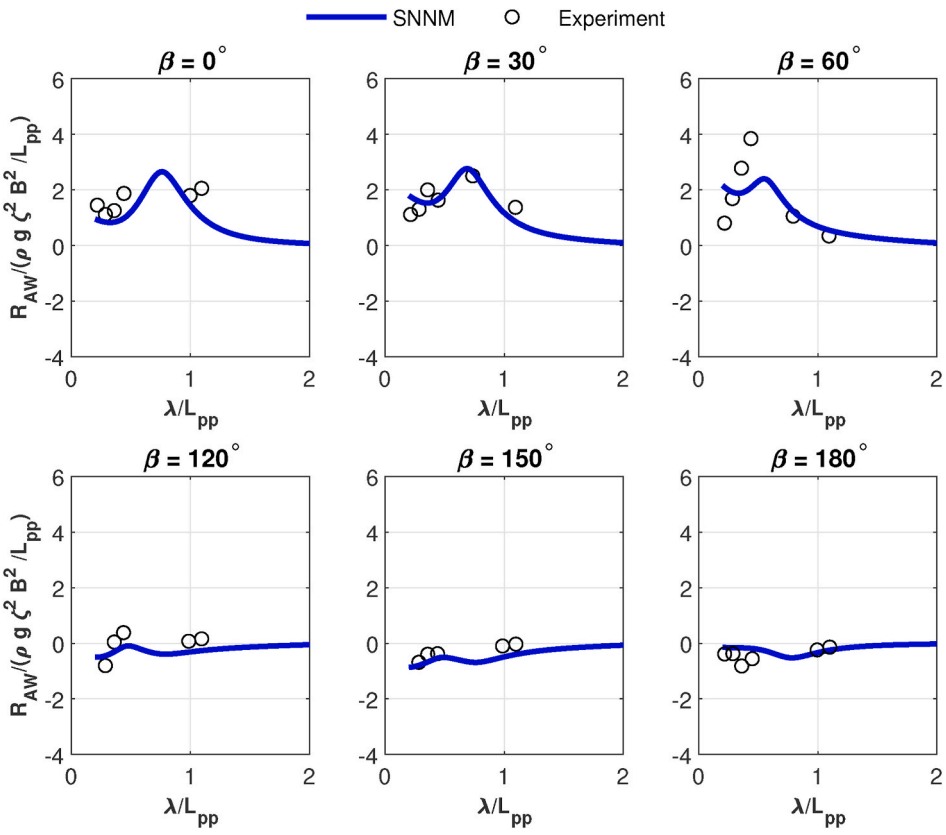

Fig. 12. Experimental and predicted added resistance of the DTC ship in design condition in regular waves with arbitrary angles at $Fr = 0.052$.

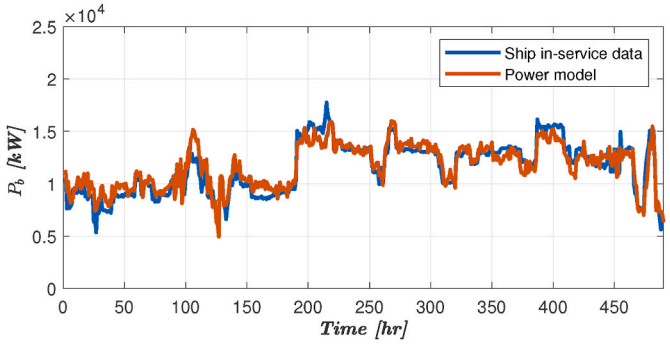

Fig. 13. Comparison of the power model against the ship in-service data of the 13100 TEU class container ship.

Table 4
Different cases studied for the problem.

Case 1: The performance of the parent ship hull, DTC container ship, in the seaway.
Case 2: Ship design using the proposed approach for the seaway.
Case 3: Designing the ship for the calm water based on the ship power profile.
Case 4: Ship design for minimum resistance at the design speed $V_d = 25$ knots, in the seaway.
Case 5: Ship design for minimum resistance at the design speed $V_d = 25$ knots in the calm water.

$= z_G + d$. Here, z_G is calculated from the parent hull such that $z_G = KG_p - d_p = 5.351$, where KG_p and d_p are equal to the vertical center of gravity and the draft of the parent hull, respectively, as presented in Table 1. This value of z_G is used for all variations of the ship in this study.

The optimization process is done through the well-known genetic algorithm (GA) by MATLAB optimization toolbox and settings presented

Table 5
Variation ranges and restrictions for the optimization problem.

	Cases 2 & 3	Cases 4 & 5
Decision variables	$6.0 \le L_{pp}/B \le 8$ $2.0 \le B/d \le 3.6$ $340 \le L_{pp}[m] \le 360$ $0.5 \le D_p/d \le 0.7$ $0.55 \le A_E/A_o \le 1.05$ $0.5 \le P/D_p \le 1.4$ $4 \le Z \le 6$	$6.0 \le L_{pp}/B \le 8$ $2.0 \le B/d \le 3.6$ $340 \le L_{pp}[m] \le 360$
Subject to	$\lvert\frac{\Delta - \Delta_0}{\Delta_0}\rvert \le 0.05$ $0.5 \le C_B \le 0.8$ $A_E/A_o \ge A_E/A_{o_{min}}$ $D_p \le 12\ m$ $GZ\ area\ (0-30deg) \ge 0.055\ m-rad$ $GZ\ area\ (0-40deg) \ge 0.09\ m-rad$ $GZ\ area\ (30-40deg) \ge 0.03\ m-rad$ $GM \ge 0.15\ m$ $Angle\ at\ GZ_{max} \ge 30\ deg$ $GZ_{max} \ge 0.2\ m$ Suez Canal limitations (Suez canal restrictions for operating, 2013) Engine limits (Section.2.5)	$\lvert\frac{\Delta - \Delta_0}{\Delta_0}\rvert \le 0.05$ $0.5 \le C_B \le 0.8$ $A_E/A_o \ge A_E/A_{o_{min}}$ $0.5 \le D_p/d \le 0.7$ $GZ\ area\ (0-30deg) \ge 0.055\ m-rad$ $GZ\ area\ (0-40deg) \ge 0.09\ m-rad$ $GZ\ area\ (30-40deg) \ge 0.03\ m-rad$ $GM \ge 0.15\ m$ $Angle\ at\ GZ_{max} \ge 30\ deg$ $GZ_{max} \ge 0.2\ m$ Suez Canal limitations (Suez canal restrictions for operating, 2013) Engine limits (Section.2.5)
Optimization objective ($\overline{F}_{Obj}$)	Maximising $\overline{V}_S$ in real sea states for Case 2 Maximising $\overline{V}_S$ in calm water for Case 3	Minimizing $\overline{R}_T$ in real sea states for Case 4 Minimizing R_{Calm} for Case 5

Table 6
GA algorithm settings.

GA Parameter	Value
Population size	40
Maximum number of generations	1000
Maximum stall generations	100
Tolerance value	0.0001
Mutation function	Constraint dependent
Selection function	Tournament

in Table 6. The optimization algorithm stops when it reaches the maximum number of generations, or the average relative change in the fitness function value over the maximum stall generations is less than Function tolerance. Further, prior to running the optimization process, the resistance criterion was checked for 100 ship hulls satisfying the decision variable limits. For the studied problem, $\sum_{k=1}^{n_{hull}} |\frac{\overline{R}_T - \overline{R}_{Calm}}{\overline{R}_T}| / n_{hull} = 0.35$ is obtained which meets the resistance criterion presented in (36).

To study the cavitation criterion over the long term, the penalty function for the cavitation for the real sea states (RSS), $\overline{P}_{Cav}^{RSS}$, is defined as follows.

$$\overline{P}_{Cav}^{RSS} = \iiiint P_{Enc}^{tot}(\beta)\, P_{SD}(H_S, T_p)\, P_P(P_b)\, I_{Cav}(\beta, H_S, T_p, P_b)\, d\beta\, dT_p\, dH_s\, dP_b \tag{39}$$

with

$$I_{Cav}^{RSS}(\beta, H_S, T_p, P_b) = \begin{cases} 1 & A_E/A_o \le A_E/A_{o_{min}} \\ 0 & \text{otherwise.} \end{cases}$$

Similarly, it is obtained for the calm water as

$$\overline{P}_{Cav}^{Calm} = \int P_P(P_b)\, I_{Cav}(P_b)\, dP_b \tag{40}$$

where

$$I_{Cav}^{Calm}(P_b) = \begin{cases} 1 & A_E/A_o \le A_E/A_{o_{min}} \\ 0 & \text{otherwise.} \end{cases}$$

To examine the engine limits, the following penalty function for real sea states is defined.

$$\overline{P}_{Eng_{lim}}^{RSS} = \iiiint P_{Enc}^{tot}(\beta)\, P_{SD}(H_S, T_p)\, P_P(P_b)\, I_{Eng_{lim}}(\beta, H_S, T_p, P_b)\, d\beta\, dT_p\, dH_s\, dP_b \tag{41}$$

with

$$I_{Eng_{lim}}^{RSS}(\beta, H_S, T_p, P_b) = \begin{cases} 1 & \textit{if engine limits are not met} \\ 0 & \text{otherwise.} \end{cases}$$

For calm water, it is given as

$$\overline{P}_{Eng_{lim}}^{Calm} = \int P_P(P_b)\, I_{Eng_{lim}^{Calm}}(P_b)\, dP_b \tag{42}$$

where

$$I_{Eng_{lim}}^{Calm}(P_b) = \begin{cases} 1 & \textit{if engine limits are not met} \\ 0 & \text{otherwise.} \end{cases}$$

During the optimization process, the cavitation and engine penalty functions are added to the optimization objective to serve as a penalty parameter for the cavitation occurrence and the breaking of the engine limits, receptively.

4. Results and discussion

Table 7 provides the results for the different cases listed in Table 5. A comparison between the underwater hull of the parent hull (Case 1) and the optimal hull (Case 2) is presented in Fig. 14. The results show that optimal hull (Case 2) is more slender than the parent hull.

Table 7
Decision variables and objectives for different cases.

Decision variables	Case 1	Case 2	Case 3	Case 4	Case 5
$L_{pp}[m]$	355.00	354.87	349.02	346.92	357.44
$B[m]$	51.00	47.24	48.16	49.42	48.41
$d[m]$	14.50	14.87	14.75	14.52	14.41
$D_p[m]$	8.91	9.08	9.06	8.91	8.91
EAR	0.80	0.72	0.86	0.80	0.80
Z	5	5	5	5	5
P/D_p	0.96	0.82	0.91	0.96	0.96
$\Delta[t]$	1.78E+05	1.70E+05	1.69E+05	1.69E+05	1.69E+05
$\overline{F}_{Obj}$	–	11.89 [knots]	15.51 [knots]	5.46E+03 [kN]	3.86E+03 [kN]
$\overline{V}_S[knots]$	10.29	11.76	10.84	10.90	10.52
$\overline{Pr}_{Cav}^{RSS}[\%]^a$	0.92	0.00	0.10	0.8	0.77
$\overline{Pr}_{Cav}^{Calm}[\%]$	0.00	0.00	0.00	0.00	0.00
$\overline{Pr}_{Eng_{lim}}^{RSS}[\%]$	33.27	0.00	27.24	28.56	34.75
$\overline{Pr}_{Eng_{lim}}^{Calm}[\%]$	0.00	0.00	0.00	0.00	0.00

[a] $\bar{Pr}_{x}^{y} = \bar{P}_{x}^{y} \times 100$.

The engine limits must be met throughout the engine's entire operating range, regardless of sea state and ship speed. Table 7 shows that while all cases meet the engine limits in the calm water condition ($\overline{Pr}_{Eng_{lim}}^{Calm} = 0$), only Case 2 meets the engine limits in all actual sea conditions. This implies that the sea margin $sm = 0.15$ assumed for calm water conditions to get the heavy running propeller curve is not sufficient to fulfill the engine requirements in the considered operational conditions. Additionally, if the ship does not meet the engine limits, its mission might not be accomplished since the captain will have to adjust the ship's speed or course to come with the limits. Assuming that the speed is changed in order to comply with the engine limits, the average ship speeds over the long term for different cases are presented in Table 7.

Based on the results, Case 2 is found to achieve a higher average operation speed over the long term (11.76 knots) thanks to its better average propulsion system efficiency $\overline{\eta}_T$ and somewhat lower average total resistance $\overline{R}_T$, as illustrated in Fig. 15a. More specifically, the results given in Table 8 indicate 14.28%, 8.48%, 7.89% and 11.79% reductions in the average ship speed $\overline{V}_S$ for Case 2 compared to cases 1, 3, 4 and 5.

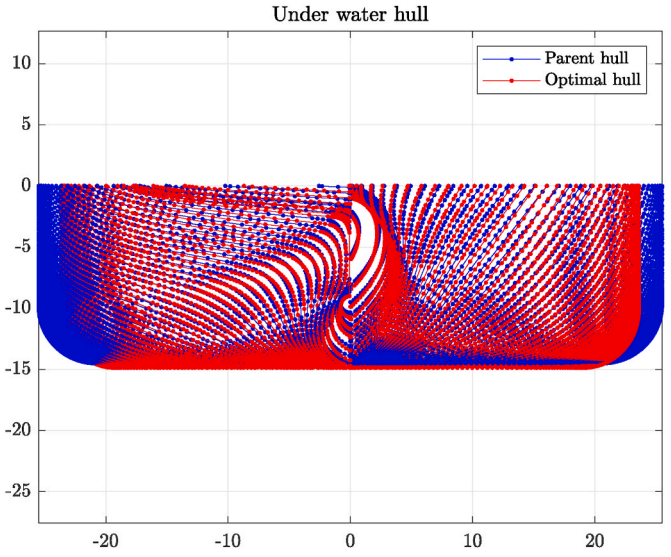

Fig. 14. Comparison of ship under water hull for the optimal hull against parent hull.

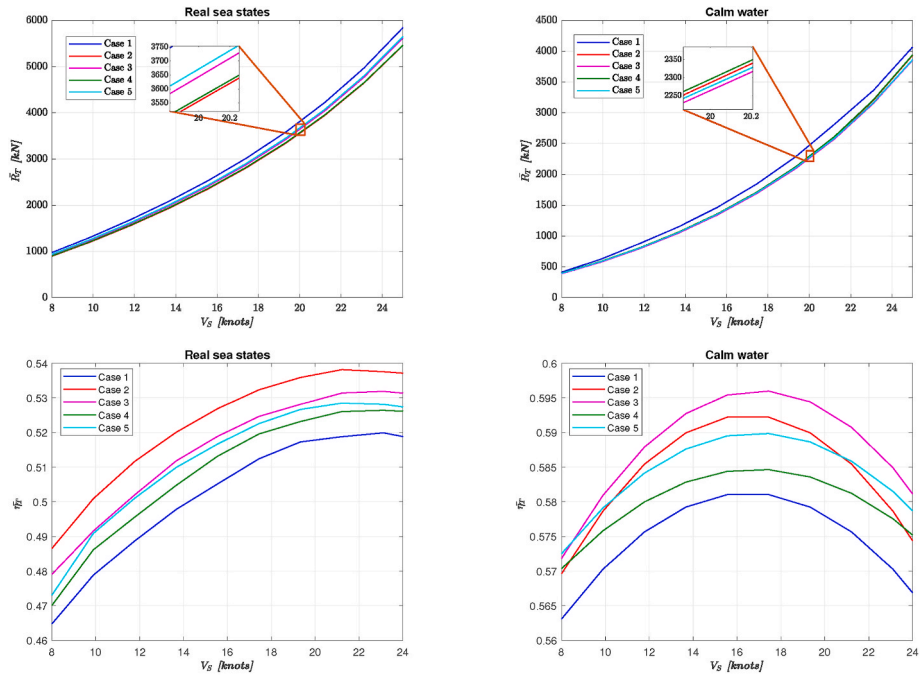

(a) Real sea state (b) Calm water

Fig. 15. The average resistance and propulsion system efficiency against ship speed for different cases.

Table 8
Percentage change (PC) of the average ship speed $\overline{V}_S$ for different cases.

	PC^a_{21}	PC_{23}	PC_{24}	PC_{25}
$\overline{V}_S$	14.28	8.48	7.89	11.79

$$^aPC_{ij} = \frac{Objective_i - Objective_j}{Objective_j} \times 100$$

Table 9
The average resistance and propulsion system efficiency of different cases at design speed.

	Real sea states		Calm water	
	$\overline{R}_T[kN]$	$\overline{\eta}_T[\%]$	$\overline{R}_T[kN]$	$\overline{\eta}_T[\%]$
Case 1	5.84E+03	51.98	4.06E+03	56.31
Case 2	5.46E+03	53.75	3.93E+03	56.96
Case 3	5.62E+03	53.19	3.86E+03	57.70
Case 4	5.46E+03	52.64	3.94E+03	56.98
Case 5	5.62E+03	52.81	3.86E+03	57.56

Fig. 15 and Table 9 further show that Case 2 has a lower average ship resistance $\overline{R}_T$ at different speeds under actual sea conditions, while the average resistance in the calm water condition is higher. In addition, $\overline{\eta}_T$ is higher for cases 2 and 3 in both real sea states and calm water conditions in most speed ranges. These results point to the importance of designing the ship for the real sea states based on her operational profile rather than just a single speed. Comparing Fig. 15a and b, it is also found that the average propulsion system efficiency $\overline{\eta}_T$ has significantly reduced in the real sea states.

In total, these results show that Case 2 has led to a better ship design in the real sea states, underscoring the importance of considering both environmental and operational effects on the ship design.

4.1. Principle particulars of propeller

The propeller's performance is heavily influenced by its diameter; a bigger propeller diameter generally means better performance. Table 7 shows that Case 2 has reached a slightly larger diameter than the other cases, resulting in a positive impact on the propulsion system efficiency.

To reach the highest efficiency, expanded area ratios need to be as low as possible, but high enough to avoid cavitation. The results show that Case 2 has a low propeller blade area ratio, while it still meets the cavitation criterion in the real sea states ($\overline{Pr}^{RSS}_{Cav} = 0$). Moreover, even though the cavitation criterion for other cases are met through the optimization algorithm for the calm water condition, the cavitation does still occur in the actual sea states. It is believed that this is due to the lower added resistance in waves, meaning that there will be less variation in propeller loading than for the cases with larger added resistance.

The number of blades plays a crucial role in preventing cavitation, vibration, and noise in the propeller. However, it also increases the propeller cost. Across all cases, the same number of blades was obtained, while the results show a decrease in P/D_p for cases 2 and 3 compared to other cases. A lower pitch allows the engine to reach its maximum rpm at a slower speed. Furthermore, an increase in pitch results in higher speeds, but slower accelerations. However, for a given speed and wake field, the optimal pitch ratio results in the highest efficiency possible. In addition, the effects of the pitch ratio on the propeller efficiency highly depend on the ship speeds and propeller loading. As a result, designing a ship based on its operational profile can mean that the propeller will experience better efficiency at different speeds and propeller loading.

4.2. Short-term analysis

The proposed approach is suggested to ensure the optimal performance of the ship during long-term operation. For the further test of the effectiveness of the suggested strategy, the ship in-service and environmental data of a similar ship (the studied 13100 TEU class container ship) is compared with the different cases studied here. The ship attainable speeds of the different cases are calculated using the same

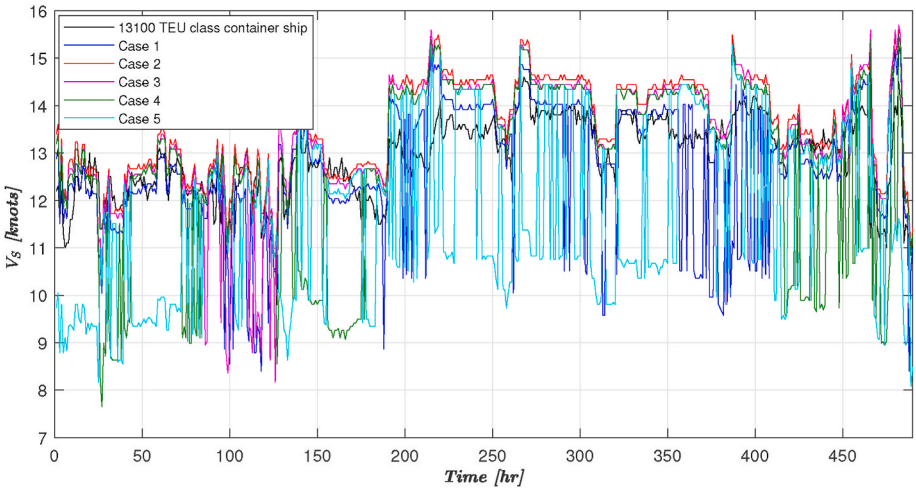

Fig. 16. Comparison of the ship speed across the 13100 TEU class container ship and studied cases.

engine power as that of the 13100 TEU class container ship in the studied environment. Fig. 16 shows the comparison for 500 h of ship attainable speeds for different cases. The sharp drops in the curves show where the ship speed has been reduced to comply with the engine limits. According to the results, Case 5 is the worst performing case in the studied scenarios, with lower speeds and more sudden changes in speeds. To avoid the frequent engine overload situations, Case 5 will need to operate at lower speeds than the intended speeds or change the route. This might prevent the ship from meeting the mission requirements. The optimal hull (Case 2) exhibits better performance and achieves higher speeds than other cases and the 13100 TEU class container ship, while satisfying the engine limits.

4.3. Ship performance in rough sea

This section compares the performance in sea states 3 (SS3) and higher of the five cases resulting from our optimization. This is done by considering the same statistical distribution of sea states as before, except that all sea states lower than SS3 are skipped from the performance evaluation. The results are presented in Tables 10 and 11, showing that the ship designed through the proposed method (Case 2) performs better than other cases. Additionally, comparing Tables 8 and 11 reveals that traditional methods have resulted in lower performances compared to the proposed strategy (Case 2) in higher sea states, demonstrating the effectiveness of the suggested approach in rough seas.

Table 10
Average ship speed for different cases at higher sea states (rough seas- SS3 and higher).

Decision variables	Case 1	Case 2	Case 3	Case 4	Case 5
$\overline{V}_S[knots]$	8.73	10.07	9.23	9.24	8.92

Table 11
Percentage Change (PC) of $\overline{V}_S$ for different cases at higher sea states (rough seas- SS3 and higher).

	PC^a_{21}	PC_{23}	PC_{24}	PC_{25}
$\overline{V}_S$	15.34	9.10	8.98	12.90

5. Conclusion

In this article, an approach was proposed for the optimal design of ships at sea. To do this, the ship power profile was obtained by analysing the ship in-service data of a similar ship operating in real sea states. The probabilities of the wave and wind encounter angles were derived by analysing both the ship in-service and hindcast data. To get the probabilities of the significant wave heights and the mean wave periods, the hindcasts data were also employed. Then, an approach based on considering the attainable average ship speed over the long term as the optimization objective was suggested. The proposed approach was tested on the DTC Post-Panamax container ship operating in a route from Busan to Hamburg. The results associated with different case studies representing the traditional methods were compared with the results of the suggested approach. Over 7.89% increase in the average ship speed over the long term was obtained. The results also reveal that ships designed based on calm water conditions with an additional sea margin of 15% meet the engine limits in approximately 70% of the encountered conditions, while the proposed approach is able to fully comply with the engine limits under all encountered conditions. This implies the importance of selecting an engine for a ship based on actual sea conditions. In addition, a comparison for the short time operation of the ship was presented, which reaffirmed the effectiveness of the result of the suggested optimization process. It was also found that the average speed in rough seas ($SS > 3$) was higher for the ship designed with the proposed optimization method. This study has used the proposed method to design a ship at the early stage. However, it could be of interest to examine the performance of the proposed approach in the detailed phases of the ship design and retrofit problems.

Although ship design is a multi-objective problem, we believe that the method proposed here can be incorporated into a holistic ship design process to provide holistic designs with improved performance in real operating conditions compared to traditional design methods. The method should be tested on different ship types and operational patterns to further explore its potential.

CRediT authorship contribution statement

Ehsan Esmailian: Conceptualization, Investigation, Methodology, Software, Writing – original draft. **Sverre Steen:** Methodology, Writing – review & editing, Supervision.

Declaration of competing interest

The authors declare that they have no known competing financial

interests or personal relationships that could have appeared to influence the work reported in this paper.

Acknowledgment

This work was carried out at SFI Smart Maritime (WP2) supported by the Research Council of Norway through the Center for Research-based Innovation (SFI) scheme (Grant number 237917). Special thanks Benjamin Lagemann for sharing his feedback regarding the proposed approach.

References

Aeberli, K., 2005. Sulzer rt-flex96c into containership service. In: Motor Ship Marine Propulsion Conference. Bilbao.
Bolbot, V., Papanikolaou, A., 2016. Optimization of ship's bow form for the added resistance in waves. In: Proc. 3rd International Conference on Maritime Technology and Engineering (MARTECH 2016), Lisbon, Portugal, pp. 611–619.
Campana, E.F., Peri, D., Tahara, Y., Stern, F., 2006. Shape optimization in ship hydrodynamics using computational fluid dynamics. Comput. Methods Appl. Mech. Eng. 196 (1–3), 634–651.
Cepowski, T., Chorab, P., 2021. Determination of design formulas for container ships at the preliminary design stage using artificial neural network and multiple nonlinear regression. Ocean Eng. 238, 109727.
Charchalis, A., Krefft, J., 2009. Main dimensions selection methodology of the container vessels in the preliminary stage. J. KONES 16, 71–78.
Copernicus climate change service. https://cds.climate.copernicus.eu/. (Accessed 8 May 2021).
Demmerle, R., 1997. Sulzer RTA84c and RTA96c Engines: the Reliable Driving Forces for Large, Fast Containerships. Technology Review, Wärtsilä NSD Switzerland Ltd.
Det Norske Veritas, 2010. Recommended Practice DNV-RP-C205: Environmental Conditions and Environmental Loads. Det Norske Veritas (DNV).
Esmailian, E., Ghassemi, H., Zakerdoost, H., 2017. Systematic probabilistic design methodology for simultaneously optimizing the ship hull–propeller system. Int. J. Nav. Archit. Ocean Eng. 9 (3), 246–255.
Esmailian, E., Gholami, H., Røstvik, H.N., Menhaj, M.B., 2019. A novel method for optimal performance of ships by simultaneous optimisation of hull-propulsion-BIPV systems. Energy Convers. Manag. 197, 111879.
Faltinsen, O.M., 1980. Prediction of resistance and propulsion of a ship in a seaway. In: Proceedings of the 13th Symposium on Naval Hydrodynamics, Tokyo, p. 1980.
Gourlay, T., von Graefe, A., Shigunov, V., Lataire, E., 2015. Comparison of AQWA, GL Rankine, MOSES, OCTOPUS, PDStrip and WAMIT with model test results for cargo ship wave-induced motions in shallow water. In: International Conference on Offshore Mechanics and Arctic Engineering, vol. 56598. American Society of Mechanical Engineers. V011T12A006.
Hart, C.G., Vlahopoulos, N., 2010. An integrated multidisciplinary particle swarm optimization approach to conceptual ship design. Struct. Multidiscip. Optim. 41 (3), 481–494.
Hollenbach, K.U., 1998. Estimating resistance and propulsion for single-screw and twin-screw ships-ship technology research 45. Schiffstechnik 45 (2), 72, 1998.
Holtrop, J., 1984. A statistical re-analysis of resistance and propulsion data. Int. Shipbuild. Prog. 31 (363), 272–276.
ISO, 2015. Ship and Marine Technology—Guidelines for the Assessment of Speed and Power Performance by Analysis of Speed Trial Data. ISO, Geneva, Switzerland.
Jinkine, V., Ferdinande, V., 1974. A method for predicting the added resistance of fast cargo ships in head waves. Int. Shipbuild. Prog. 21 (238), 149–167.
Joung, T.-H., Kang, S.-G., Lee, J.-K., Ahn, J., 2020. The IMO initial strategy for reducing greenhouse gas (GHG) emissions, and its follow-up actions towards 2050. J. Int. Marit. Saf. Environ. Affairs. Ship. 4 (1), 1–7.
Jung, Y.-W., Kim, Y., 2019. Hull form optimization in the conceptual design stage considering operational efficiency in waves. Proc. IME M J. Eng. Marit. Environ. 233 (3), 745–759.
Kim, B.-S., Oh, M.-J., Lee, J.-H., Kim, Y.-h., Roh, M.-I., 2021. Study on hull optimization process considering operational efficiency in waves. Processes 9 (5), 898.
Kramer, M., Motley, M., Young, Y., 2010. Probabilistic-based design of waterjet propulsors for surface effect ships. In: Proceedings of the 29th American Towing Tank Conference. ATTC.
Larsson, L., Janson, C., Broberg, L., Regnström, B., 2020. Shipflow 6.5 User Manual. FLOWTECH International AB, Gothenburg, Sweden.
Lee, C.-M., Yu, J.-W., Choi, J.-E., Lee, I., 2019. Effect of bow hull forms on the resistance performance in calm water and waves for 66k dwt bulk carrier. Int. J. Nav. Archit. Ocean Eng. 11 (2), 723–735.
Liu, S., Papanikolaou, A., 2020. Regression analysis of experimental data for added resistance in waves of arbitrary heading and development of a semi-empirical formula. Ocean Eng. 206, 107357.
MAN Energy Solutions, 2018. Basic Principles of Ship Propulsion. MAN Energy Solutions.
Moctar, O.e., Shigunov, V., Zorn, T., 2012. Duisburg test case: post-panamax container ship for benchmarking. Ship Technol. Res. 59 (3), 50–64.
Motley, M.R., Young, Y.L., 2011. Performance-based design and analysis of flexible composite propulsors. J. Fluid Struct. 27 (8), 1310–1325.
Motley, M.R., Nelson, M., Young, Y.L., 2012. Integrated probabilistic design of marine propulsors to minimize lifetime fuel consumption. Ocean Eng. 45, 1–8.
Nelson, M., Temple, D., Hwang, J.T., Young, Y.L., Martins, J., Collette, M., 2013. Simultaneous optimization of propeller–hull systems to minimize lifetime fuel consumption. Appl. Ocean Res. 43, 46–52.
Oosterveld, M.W.C., van Oossanen, P., 1975. Further computer-analyzed data of the Wageningen B-screw series. Int. Shipbuild. Prog. 22 (251), 251–262.
Perez, T., Smogeli, O., Fossen, T., Sorensen, A., 2006. An overview of the marine systems simulator (mss): a simulink toolbox for marine control systems. Model. Ident. Control 27 (4), 259–275.
Peri, D., Rossetti, M., Campana, E.F., 2001. Design optimization of ship hulls via cfd techniques. J. Ship Res. 45 (2), 140–149.
Radan, D., 2008. Integrated Control of Marine Electrical Power Systems, PhD Thesis, Fakultet for Ingeniørvitenskap Og Teknologi. NTNU.
Resolution, M., 2018. 304 (72) initial IMO strategy on reduction of GHG emissions from ships. MEPC 72, 17.
Serani, A., Diez, M., Leotardi, C., Peri, D., Fasano, G., Iemma, U., Campana, E.F., 2014. On the use of synchronous and asynchronous single-objective deterministic particle swarm optimization in ship design problems. In: Proceeding of OPT-I, International Conference on Engineering and Applied Sciences Optimization. Kos Island, Greece.
Smith, T.W., Jalkanen, J., Anderson, B., Corbett, J., Faber, J., Hanayama, S., O'keeffe, E., Parker, S., Johansson, L., Aldous, L., et al., 2014. Third IMO Greenhouse Gas Study.
Smogeli, Ø.N., 2006. Control of Marine Propellers: from Normal to Extreme Conditions, PhD Thesis, Fakultet for Ingeniørvitenskap Og Teknologi. NTNU.
Smogeli, Ø.N., Sørensen, A.J., 2009. Antispin thruster control for ships. IEEE Trans. Control Syst. Technol. 17 (6), 1362–1375.
Smogeli, Ø.N., Sørensen, A.J., Minsaas, K.J., 2008. The concept of anti-spin thruster control. Control Eng. Pract. 16 (4), 465–481.
Sørensen, A.J., Smogeli, Ø.N., 2009. Torque and power control of electrically driven marine propellers. Control Eng. Pract. 17 (9), 1053–1064.
Stewart, R.H., 2008. Introduction to Physical Oceanography. Internet Archive.
Suez canal restrictions for operating ships. https://web.archive.org/web/20130604114747/http://www.suezcanal.gov.eg/Files/2-2010.pdf. (Accessed 8 May 2021).
Temple, D., Collette, M., 2012. Multi-objective hull form optimization to compare build cost and lifetime fuel consumption. In: International Marine Design Conference. IMDC, Glasgow, Scotland, pp. 11–14.
Wang, J., Bielicki, S., Kluwe, F., Orihara, H., Xin, G., Kume, K., Oh, S., Liu, S., Feng, P., 2021. Validation study on a new semi-empirical method for the prediction of added resistance in waves of arbitrary heading in analyzing ship speed trial results. Ocean Eng. 240, 109959.
Yeginbayeva, I., Atlar, M., 2018. An experimental investigation into the surface and hydrodynamic characteristics of marine coatings with mimicked hull roughness ranges. Biofouling 34 (9), 1001–1019.